International Journal of Physical Sciences Vol. 7(24), pp. 3073 - 3081, 22 June, 2012
Available online at http://www.academicjournals.org/IJPS
DOI: 10.5897/IJPS12.230
ISSN 1992 - 1950 ©2012 Academic Journals

Full Length Research Paper

Impact of frequency switching on the efficiency of a fully suspended active magnetic bearing system

Rupert Gouws

Faculty of Engineering, North-West University, Potchefstroom, 2522, South Africa. E-mail: Rupert.Gouws@nwu.ac.za.

Accepted 14 May, 2012

Due to the rising energy (and electricity) cost it is essential that an active magnetic bearing (AMB) system is operated as efficiently as possible. Frequency switching caused by an external source can cause an AMB system to operate at a higher than expected energy level and lower than expected efficiency. The purpose of this paper is therefore to investigate the impact of frequency switching (caused by an external source) on the efficiency of a fully suspended AMB system. The shaft of the fully suspended AMB system for this project is mechanically connected and driven by an induction motor and the vertical and horizontal displacements of the driven unit are controlled by means of PID controllers. The model of the fully suspended AMB system with the external fault and the process diagram used for frequency extraction during the fault condition is presented. It is shown that the efficiency of the fully suspended AMB system can be improved by optimizing the controller performance during the external fault condition.

Key words: Active magnetic bearings, efficiency and vibration analysis, induction motor, external faults.

INTRODUCTION

An electromagnetic device which levitates a rotor by controlling the attractive electromagnetic forces can be seen as an active magnet bearing (AMB). AMBs are used in the industry due to the fact that there is no mechanical contact between the parts, no lubrication requirements and high-precision operation (Agarwal et al., 2009; Gouws et al., 2011; Kim et al., 1999).

AMB systems can further be seen as modern mechatronical systems and have the advantage of high life time and low maintenance cost (Khoo et al., 2010; Ritonja et al., 2006; Schweitzer et al., 1993).

The use of magnetic bearings in turbo-machinery, pumps, compressors, motors and generators has strongly increased over the last few years, since users expect that their machines are running safe and reliable and that they have high efficiency and availability (Gopalakrishan, 1999; Nordmann et al., 2004).

The performance of the power amplifiers, as part of the electronic control system of the AMB system directly affects the suspension system and overall performance of the AMB system. The power amplifiers are therefore a crucial component of the AMB system (Lei, 2011).

In this paper the impact of frequency switching (caused by an external source) on the efficiency of a fully suspended AMB system is analysed and presented. As part of the analysis process the rotor displacement and current from the power amplifiers are used to identify the external fault component. It is further shown that the efficiency of the AMB system can be improved by optimizing the performance of the PID controllers.

The materials and method used during this project is presented in detail and the efficiency analysis results obtained from the AMB system is also presented. Finally, a conclusion on the results obtained from the frequency extraction of the external fault component is drawn.

MATERIALS AND METHODS

This section provides an overview on the fully suspended AMB system and the method used to determine the impact of frequency switching (caused by an external source) on the efficiency of the AMB system. Figure 1 provides the experimental setup of the AMB system with the external fault. From Figure 1, it can be seen that the driven unit is fully suspended by means of axial and radial magnetic bearings. The driven unit is connected to the rotor of the

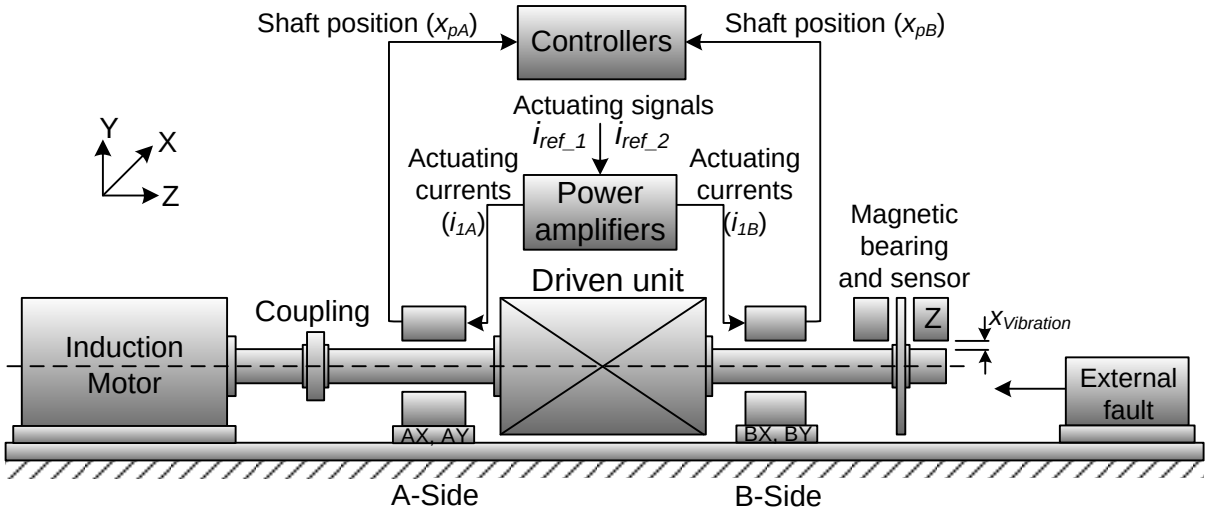

Figure 1. Experimental setup of the AMB system with the external fault.

AMB system and forms part of the water pumping system. Sensors are positioned to measure the rotor displacement of the AMB system in all three axes. The measured shaft position (x_{pA} and x_{pB}) are send to a controller, which in turn provides actuating signals (i_{ref_1} and i_{ref_2}) for the power amplifiers. A PID controller is used to provide reference actuating signals for the power amplifiers. The parameters of the PID controller are calculated according to the normal operating condition of the fully suspended AMB system without an external fault condition.

The power amplifier provides the magnetic bearings with actuating current (i_{1A} and i_{2A}). The AMB system is driven by an induction motor which is mechanically connected to the shaft by means of a coupling. The mechanical coupling has an influence on the dynamic behaviour of the rotor of the AMB system. The method however been followed in this paper to perform frequency extraction focus specifically on the difference between the normal operating condition and the external fault operated condition. For this project the mechanical coupling must be the same for both scenarios and is therefore seen (chosen) as a constant loss on the AMB system.

The induction motor is a three-phase, 50 Hz, 380 V, industrial scale induction motor with a squirrel cage rotor and is speed controlled by means of a variable speed drive (VSD). An external fault caused by an external source with a frequency switching capability causes disturbance on the shaft of the AMB system. The external fault is caused by a power PROFET PWM motor driver which is used to drive a DC motor in the same vicinity as the fully suspended AMB system. More detail and specifications on the fully suspended AMB system is provided by Gouws et al. (2011).

A simulation model of the AMB system which provides the rotor displacement and power amplifier currents (which is already available from the practical AMB system) will be used during the analysis and frequency extraction of the external fault component. More detail on active magnetic bearings for machining applications is provided by Knospe (2007).

To observe how the practical AMB model will respond to faults, a Matlab® Simulink® simulation model of the AMB system with the external fault condition was designed, as shown in Figure 2. From Figure 2, the displacement error (e_p) is obtained by subtracting the actual displacement (x_p) from the reference displacement (x_{pref}) which is provided by the DSP wave generator. The displacement error (e_p) is fed to a discrete PID controller, which together with the bias current (i_0) provides the reference currents (i_{ref_1} and i_{ref_2}) for the power amplifier. Current function blocks together with saturation limiter blocks are used to calculate the actual power amplifier currents (i_1 and i_2). The top and bottom forces exerted on the AMB system are calculated from $(K_m \cdot i_1^2)/x_p^2$ and $(K_m \cdot i_2^2)/(x_{pref} - x_p)^2$, where K_m represents the constant value for the magnetic bearing.

The force f_3 represents the carrier force ($f_3(\omega_1 t)$) on the AMB system and the fault condition subsystem represents the external fault condition with the frequency switching component on the AMB system. The external fault condition is simulated by means of vibration forces (f_4) which are synchronously placed on the carrier of the AMB system. More detail on the process regarding the modulation and demodulation of reference forces and the placement of the vibration forces on the AMB system is provided by Gouws et al. (2009).

The rotor displacement (x_p) is obtained by subtracting the gravitation force from the remaining forces, dividing the answer by the mass of the rotor (m) and by using two discrete-time integrator function blocks. Noise and saturation limits are added to the signal to more closely represent the practical system.

A voltage function subsystem together with a saturation limiter block provides the actual power amplifier voltage (v_1). The RMS active and reactive power of the power amplifiers are then calculated by means of the discrete active and reactive power block and DRMS blocks.

To obtain a filtered DFT signal from the current data of the power amplifiers, the current is fed through a model comparison subsystem, DFT function block and filtering subsystem. The frequency extraction process for the external fault component is further explained in Figure 3.

The results on the AMB system is for a PID controlled system, since the physical working water cooling AMB system is currently been operated by PID controllers. The focus was to investigate the influence of external frequency switching on the efficiency of the physical working water cooling AMB system. Sliding mode controllers and logic flow controllers can be used as an alternative to PID controllers, but falls outside the scope of this paper. More detail on robust control of an active magnetic bearing subject to voltage saturation is provided by Du et al. (2010).

Figure 3 provides the process diagram that was used for

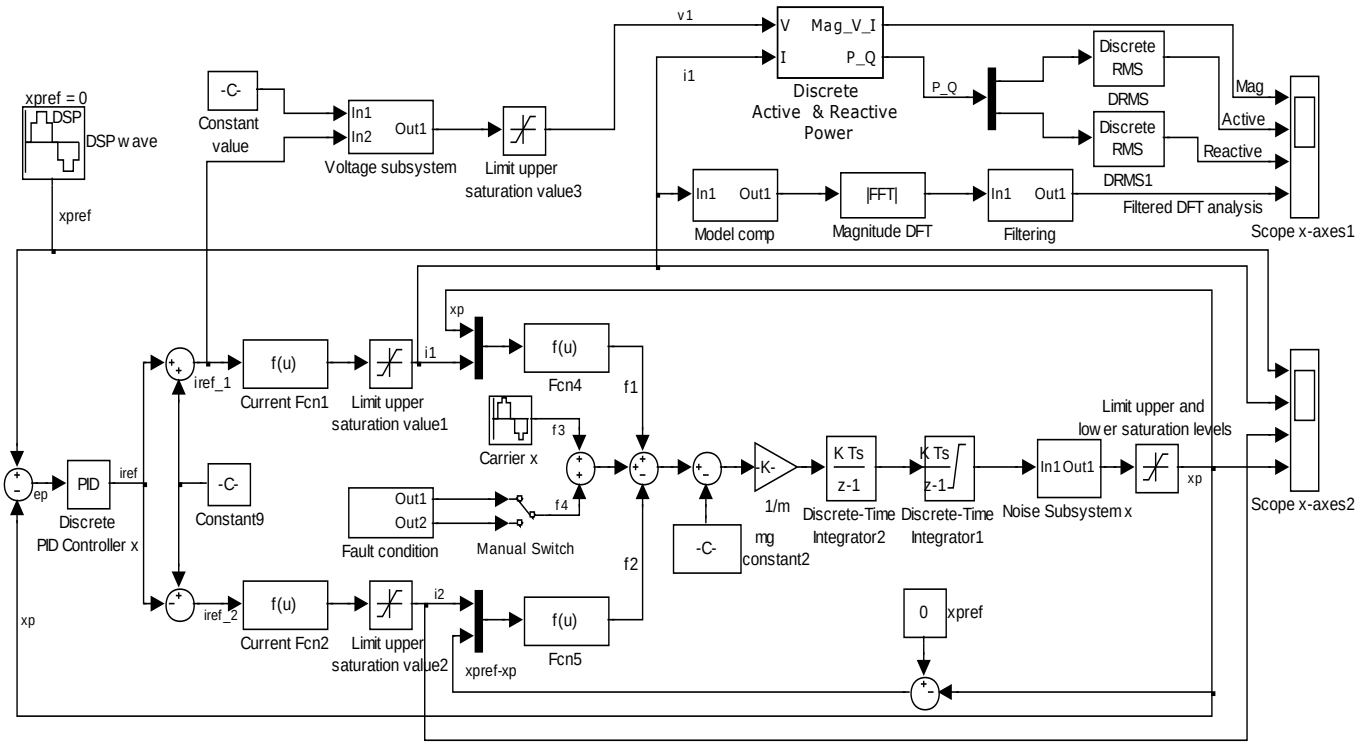

Figure 2. Matlab® Simulink® model of the AMB system with the external fault.

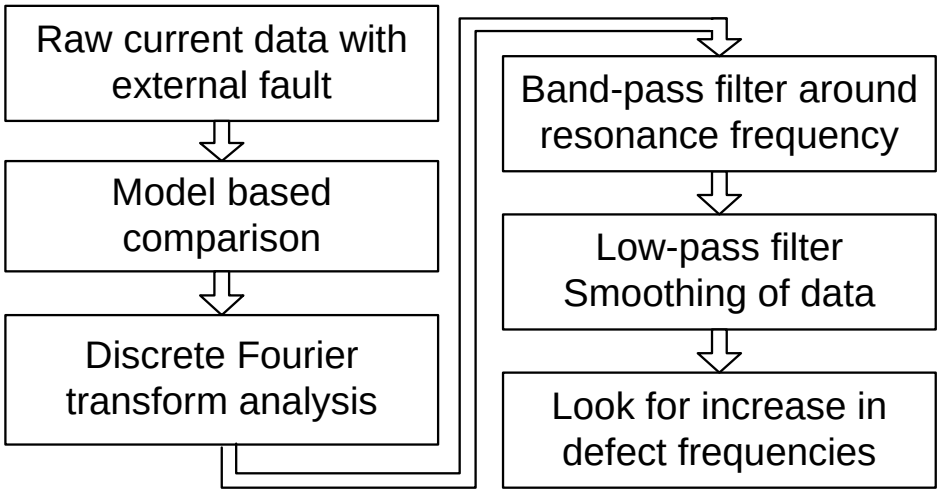

Figure 3. Process diagram used for frequency extraction of the external fault component.

frequency extraction of the external fault component. The raw current data from the power amplifier with the external frequency fault component is compared to an ideal model based current with no fault component, during model based comparison. The discrete Fourier transform (DFT) analysis is performed after model based comparison on the difference signal. The DFT signal is then band-pass filtered around the resonance frequency and low-pass filtered to smooth the data. The external fault component is then analysed in the frequency spectrum and any increases in the defect frequencies are clearly visible. More detail on the detecting of cracked rotors using auxiliary harmonic excitation is provided by Sawicki et al. (2011).

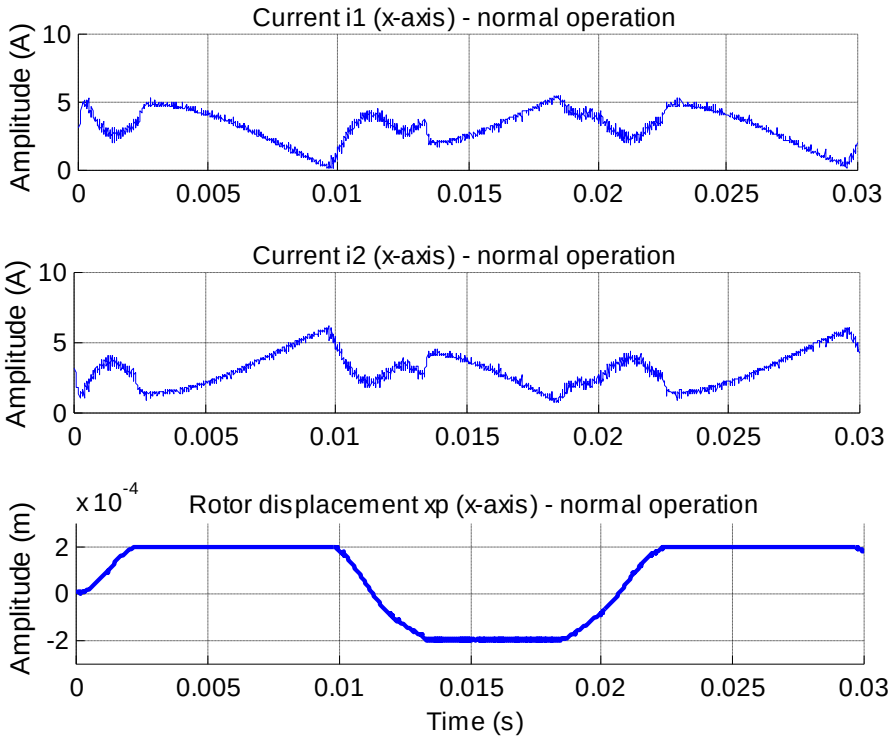

Figure 4. Current and rotor displacement during normal operation.

RESULTS AND DISCUSSION

This section provides the results obtained from the fully suspended AMB system with the external fault condition. The Matlab® Simulink® model as explained as shown in Figure 2 was used as basis to obtain the results. Also, results on the power amplifier current (for the top and bottom magnetic bearings) and rotor displacement during normal (or ideal) operation and during the external fault condition are provided.

An analysis is then provided on the active power and cumulative active power for the normal condition and fault condition. An efficiency analysis of the AMB system for the normal operation and fault condition with different proportional gain values are then provided. The results obtained from the frequency extraction of the external fault component are then provided.

Figure 4 provides a graph of the current and rotor displacement during normal operation (or no fault operation) of the AMB system. From Figure 4 it can be seen that the current for the top power amplifier (current i1) and current for the bottom power amplifier (current i2) peaks around 5 A. The current for the bottom power amplifier is an inverse to that of the top power amplifier. The rotor displacement (x_p) varies between 0.0002 and -0.0002 mm. The unbalance default is normally visible in the rotor displacement of the AMB system. For the efficiency analysis results and frequency analysis results (of the experimental results) the unbalance default has been removed. The unbalance default is seen as a constant force (with a specific frequency component) on the rotor of the AMB system. This constant component has been removed, since it has no influence on the efficiency and frequency analysis been done and the component value is the same for both scenarios.

Figure 5 provides a graph of the current and rotor displacement during the fault condition. From Figure 5 it can be seen that the current of the top and bottom power amplifiers again peaks around 5 A, but an addition switching frequency component is visible in the current signals. The same switching frequency component is visible in the rotor displacement of the AMB system. The current of the bottom power amplifier is again an inverse to the current of the top power amplifier.

Figure 6 provides a graph of the cumulative active power during normal operation and the fault condition. From Figure 6, it can be seen that the active power during fault condition peaks above 2000 W, whereas the active power during normal operation stays below 2000 W. The cumulative active power during the fault condition is also higher compared to the normal (or ideal) operation.

Figure 7 provides a graph of the efficiency decrease of the AMB system with proportional gain increase during

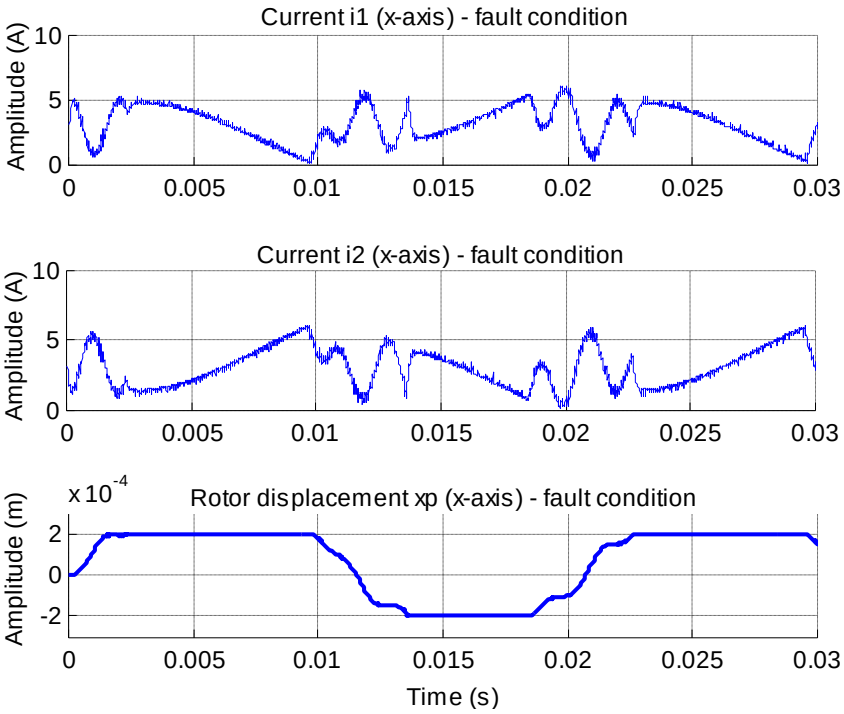

Figure 5. Current and rotor displacement during the fault condition.

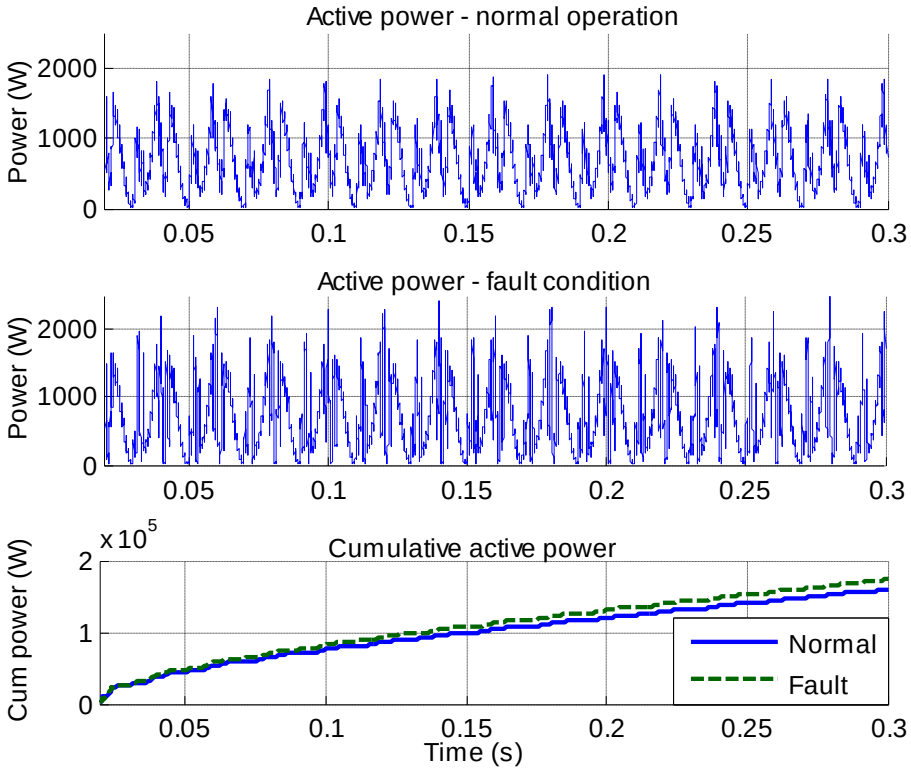

Figure 6. Cumulative active power during normal operation and the fault condition.

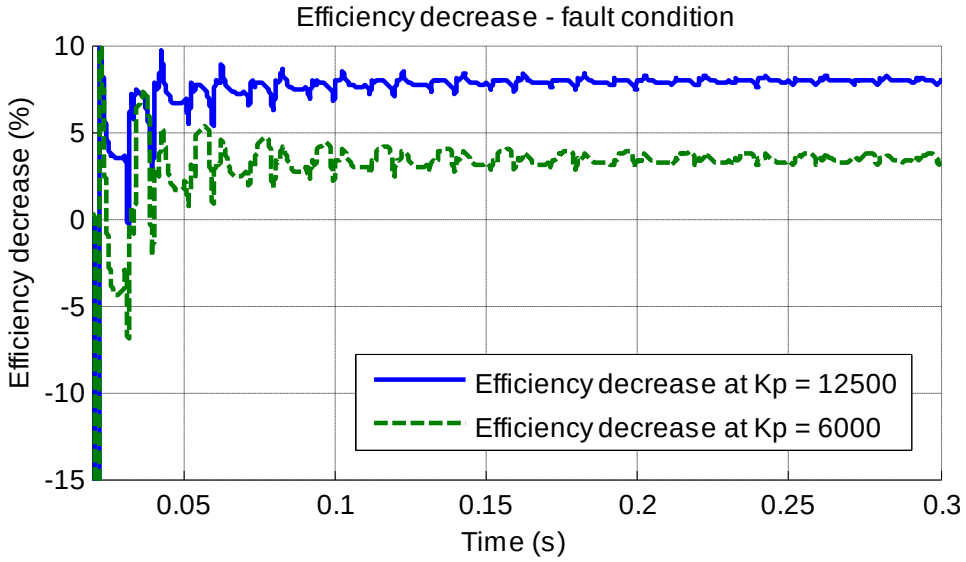

Figure 7. Efficiency decrease with proportional gain increase during the fault condition.

the fault condition. From Figure 7, it can be seen that when the proportional gain (K_p) is 12500, the decrease in efficiency is higher compared to a proportional gain of 6000. The proportional gain value of 12500 is mathematically calculated to be the optimal value for this specific AMB system under no fault condition. The external fault condition however causes additional stress on the displacement of the AMB rotor (which causes the power amplifiers to work harder), which can be relieved by lowering the gain values of the PID controller. This in turn causes a lowering in the efficiency decrease component for this specific AMB system. More detail on the control and parameter selection of an AMB system is provided by Gouws et al. (2009).

Table 1 provides the data obtained from the efficiency analysis of the AMB system with the external fault condition. In Table 1, a decrease in efficiency represents the difference in the efficiency from the normal (ideal) operation to the external fault condition, whereas an improvement in efficiency from optimal represents the improvement in the efficiency from the optimal value of 12500. From Table 1, it can be seen that when the proportional gain (K_p) is low (6000) the decrease in efficiency is also low (3.349%) and the efficiency improvement from optimal is 4.497%, under external fault conditions. When the proportional gain is increase to 15000 the decrease in efficiency also increases to 11.460% and the efficiency improvement from optimal is -3.500%, under external fault conditions. The efficiency of the AMB system can therefore be improved from optimal by lowering the proportional gain value from 12500 (which is the optimal value) to 6000. When the proportional gain value is lowered from 6000 to 5000, the improvement in the efficiency from the optimal value decreases from 4.611 to 4.497%. This decrease in the efficiency improvement is a result of the AMB system becoming unstable due to a very low proportional gain value.

Figure 8 provides a graph of the efficiency decrease of the AMB system against the proportional gain. From Figure 8 it can be seen that the data follows a second order polynomial of $y = 9x10^{-8}x^2 - 0.0009x + 5.8545$ with a R^2 value of 0.9991. It is shown that when the proportional gain (K_p) value is lowered under external fault condition the efficiency decrease value can be lowered. The R^2 value obtained for the fit between the measured data and the second order polynomial represents a very good fit. More detail on second order polynomial line fittings (or trend-lines) and the coefficient of determination (R^2) are provided by Griffiths (2006).

Figure 9 provides a graph of the frequency analysis during the external fault condition after the filtering process. The data presented in Figure 9 is the result obtained from the frequency extraction process, as described in Figure 3. From Figure 9 it can be seen that a single frequency component with amplitude of 56.988 dB and frequency of 494 Hz has been isolated after the frequency extraction process. Noise around the isolated component has been filtered.

Figure 10 provides a graph of the orbital representation (stability analysis) of the displacement of the rotor of the AMB system under normal operating conditions. The blue ring closest to the centre is the x-axes and y-axes displacement orbital of the AMB system. A stability

Table 1. Efficiency analysis of the AMB system with the fault condition.

Proportional gain (K_p)	Efficiency decrease (%)	Efficiency improvement from optimal (%)
5000	3.463	4.497
6000	3.349	4.611
7000	3.448	4.512
8000	3.838	4.122
9000	4.456	3.504
10000	5.256	2.704
11000	6.224	1.736
12000	7.336	0.624
12500	7.960	Optimal
13000	8.584	-0.624
14000	9.960	-2.000
15000	11.460	-3.500

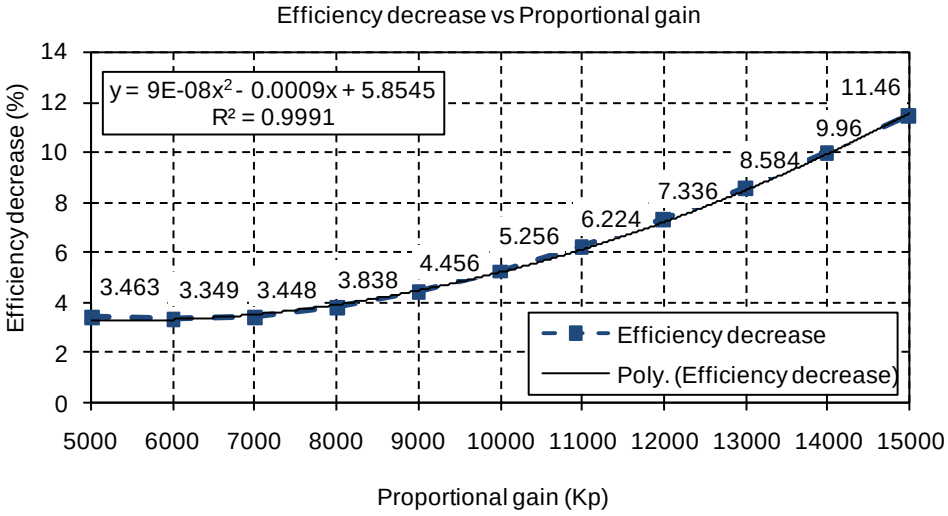

Figure 8. Efficiency decrease of the AMB system against the proportional gain.

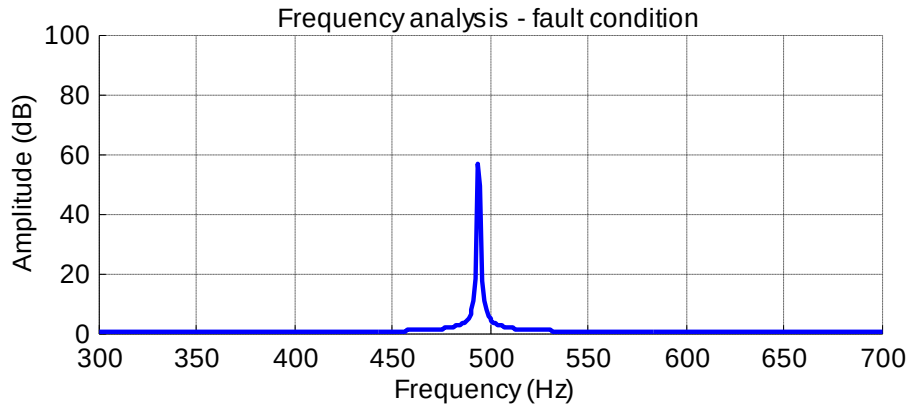

Figure 9. Frequency analysis during the fault condition after filtering.

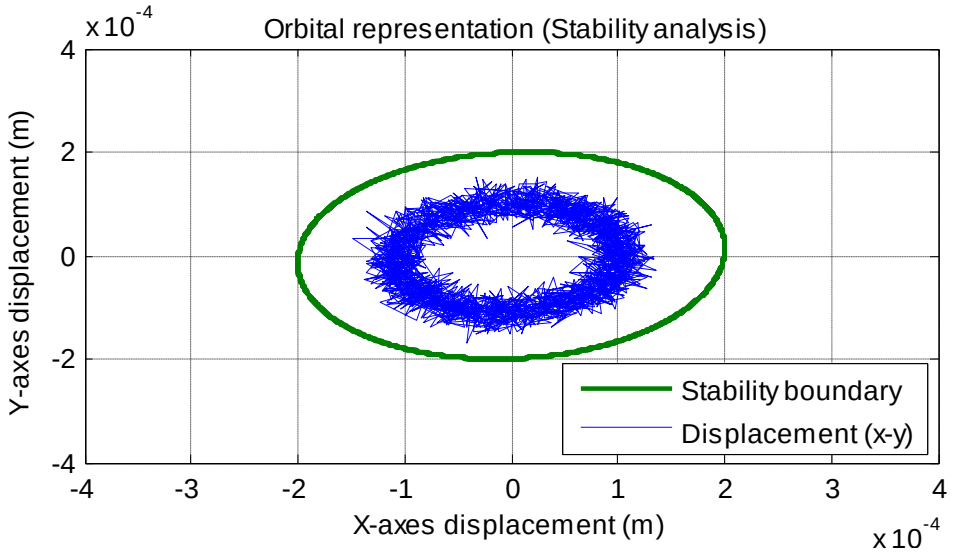

Figure 10. Orbital representation (stability analysis).

boundary has been included on the same graph. From Figure 10, it can be seen that the rotor operates within the provided stability margin (boundary) and that the orbit described by the rotor centre provides additional information on the dynamics (and stability of the rotor) for this experimental setup.

Conclusion

In this paper the impact of external frequency switching on the efficiency of a fully suspended AMB system was investigated and presented. It is shown that the cumulative active power during the external fault condition is higher compared to the normal ideal operation of the AMB system.

It is shown from the efficiency analysis that the external fault condition causes additional stress on the displacement of the AMB rotor which in turn causes the power amplifiers to work harder. This additional stress can however be relieved by lowering the proportional gain value of the PID controller, which will in turn increase the efficiency of the AMB system. It is therefore shown that the efficiency of the AMB system can be improved by optimizing the controller performance.

It is shown from the frequency analysis that a single frequency component with amplitude of 56.988 dB and frequency of 494 Hz has been isolated after the frequency extraction process. It is estimated that this specific external frequency component is caused by a power PROFET (transistor BTS 555) PWM motor driver which is switching at 500 Hz. The PROFET is used to drive a DC motor and is installed in the same area as the AMB system.

A solution to the problem is to isolate the AMB system from external noise by installing shielded cables and by shielding all switching motor drives to minimize the effect of external noise on the AMB system. More detail on the effect of controllers on the dynamic behaviour of a rotor supported on active magnetic bearings is provided by Ding et al. (2010).

REFERENCES

Agarwal PK, Chand S (2009). Fault-tolerant control of three-pole active magnetic bearing. Int. J. Exp. Sys. App., 36: 12592-12604.
Ding W, Changsheng ZHU, Ming T, Bin Z (2010). The effect of controllers on the dynamic behaviour of a rotor supported on active magnetic bearings. Int. Conf. on Elect. Contr. Eng., 1: 2336-2339.
Du H, Zhang N, Ji JC, Gao W (2010). Robust fuzzy control of an active magnetic bearing subject to voltage saturation. IEEE Trans. Contr. Sys. Tech., 18: 164-169.
Gopalakrishan S (1999). Pump research and development: Past, present and future. J. Fluids Eng., 121: 237-248.
Gouws R, van Schoor G (2009). Multiple frequency fault detection, correction and identification of vibration forces on the rotor of a rotational active magnetic bearing system. Afr. Res. J., 99: 114-123.
Gouws R, van Schoor G (2011). Real-time displacement analysis and correction system for vibration forces on rotor of rotational active magnetic bearing system. World J. Eng., 8: 381-394.
Griffiths IW (2006). Principles of biomechanics and motion analysis. Lippincott Williams & Wilkins.
Khoo WKS, Kalita K, Garvey SD (2010). Active axial-magnetomotive force parallel-airgap serial flux magnetic bearings. IEEE Trans. on Magn., 46: 2596-2602.
Kim S, Lee C (1999). Diagnosis of sensor faults in active magnetic bearing system equipped with built-in force transducers. IEEE/ASME Trans. on Mech., 4: 180-186.
Knospe CR (2007). Active magnetic bearings for machining applications. Contr. Eng. Pract., 15: 307-313.
Lei H, Ying C, Peng H (2011). Design of PWM switching power amplifier for active magnet bearing. Energy Proc., 11: 1942-1946.
Nordmann R, Aenis M (2004). Fault diagnosis in a centrifugal pump

using active magnetic bearings. Int. J. Rot. Mach., 10: 183-191.
Ritonja J, Polajzer B, Dolinar D (2006). Decentralized control for active magnetic bearings. Int. Pow. Elect. Mot. Contr. Conf. (EPE-PEMC), 12: 1413-1418.
Sawicki JT, Friswell MI, Kules Z, Wroblewski A, Lekki JD (2011). Detecting cracked rotors using auxiliary harmonic excitation. J. Sound and Vibr., 330: 1365-1381.
Schweitzer G, Traxler A, Bleuler H (1993). Magnetlager, grundlagen, eigenschaften und anwendungen berührungsfreier, elektromagnetischer Lager. Springer Verlag, Berlin, pp. 1-17